

# Research on Reactive Power Control Strategy for Small Extinction Angle Operation of Hybrid Commutation Converters

Jiaying Ning, Xiaoguang Wei, Zhichang Yuan, Longlong Chen, Hui Du, and Zhanqing Yu

**Abstract**—Hybrid commutation converters (HCCs) utilizing reverse-blocking integrated gate commutation thyristors (IGCTs) have gained significant attention due to their immunity to commutation failure. Leveraging the recovery enhancement characteristics of IGCTs, HCCs demonstrate superior performance at reduced extinction angles, thereby minimizing reactive power consumption. This study presents a comprehensive investigation into reactive power control strategies for HCCs operating at small extinction angles. First, the topological configuration and commutation principle of HCC are elucidated. Subsequently, the mechanism of HCC reactive power control is analyzed, and a reactive power control strategy is proposed by combining the converter transformer taps with extinction angles. Moreover, the relationship between transformer taps and reactive power exchange under different rated extinction angles is calculated, and the theoretically rated extinction angle is proposed. Finally, to validate the proposed control strategy, a four-terminal ultra-high voltage direct current power grid incorporating HCC technology is modeled and simulated using PSCAD/EMTDC. The simulation results demonstrate that the proposed strategy effectively supports AC systems by reducing reactive power absorption in HCCs, while simultaneously exhibiting enhanced reliability and economic efficiency.

**Index Terms**—Commutation failure, extinction angle, HCC, reactive power, tap position.

## I. INTRODUCTION

With the continuous promotion of the “carbon peaking, carbon neutrality” goals, energy transformation is becoming increasingly intense [1]. Large-scale development and utilization of renewable energy, such as solar and wind energy, becomes an inevitable trend. However, in China, a significant geographical disparity exists between renewable energy resources and load centers [2], necessitating the adoption of high voltage direct current (HVDC) transmission technology as an essential solution for efficient renewable energy integration [3]. Among HVDC technologies, line commutated converter-based HVDC (LCC-HVDC) is a predominant solution for large-capacity, long-distance power transmission, owing to its superior voltage tolerance and high-power transmission capabilities [4]. Nevertheless, since thyristors used in LCC are semi-controlled devices, the commutation of LCC relies on the connected AC grid voltage [5]. Therefore, commutation failure (CF) may occur when there is a fault in the AC grids, which has become a key factor restricting the reliability of LCC.

The root cause of CF problem stems from the inherent uncontrollable turn-off characteristic of thyristors. In contrast, voltage source converter-based HVDC (VSC-HVDC) using fully-controlled insulated-gate bipolar transistor (IGBT) does not have CF problem [6]. However, due to the limitation of the current carrying capacity of IGBTs, VSC-HVDC is restricted in terms of maximum transmission capacity and distance [7]. Therefore, it is urgent to explore a new type of semiconductor device that combines the advantages of thyristors and IGBTs to compensate for the shortcomings of existing HVDC technologies.

With the development of high-power semiconductor technology, reverse-blocking integrated gate commutation thyristors (IGCTs) have emerged, which combine high voltage resistance, big transmission power, strong controllability, etc. [8]–[11]. IGCTs can provide device-level support for the development of novel converter technologies, e.g., the hybrid commutated converter

---

Received: February 10, 2025

Accepted: November 3, 2025

Published Online: January 1, 2026

Jiaying Ning, Xiaoguang Wei (corresponding author), Longlong Chen, and Hui Du are with Beijing Huairou Laboratory, Beijing 102209, China (e-mail: ningjiaying@neps.hrl.ac.cn; weixiaoguang@neps.hrl.ac.cn; chenlong\_003@163.com; duhui@neps.hrl.ac.cn).

Zhichang Yuan and Zhanqing Yu are with Beijing Huairou Laboratory, Beijing 102209, China; and also with the Department of Electrical Engineering, Tsinghua University, Beijing 100084, China (e-mail: yuanzc@mail.tsinghua.edu.cn; yzq@tsinghua.edu.cn).

DOI: 10.23919/PCMP.2024.000365

(HCC) adopts IGCT devices, utilizing the controllable turn-off performance of IGCTs [12]. This technological integration effectively addresses the CF issue while maintaining suitability for large-capacity, long-distance power transmission [13].

China is currently planning the world's first demonstration project for large-scale renewable energy transmission through a multi-terminal ultra-high voltage direct current (UHVDC) system [14], marking a significant milestone in power transmission technology. Furthermore, HCC is being actively considered for implementation at the receiving end of the multi-terminal UHVDC power grid. IGCTs used by HCC have recovery enhancement characteristics [15]. During natural commutation, the time for IGCTs to restore their blocking ability after the current crosses zero is shorter than that of thyristors [16]. Compared to LCC, HCC has the potential to operate at smaller extinction angles, thereby reducing reactive power demand. This advantage is particularly valuable in UHVDC applications, where operating at smaller extinction angles offers significant economic benefits. In the context of new device characteristics, it is important to study reactive power control strategies suitable for small extinction angle operation of HCC.

As HCC is a relatively recent technological development, there only has been limited research on its reactive power control strategies. Current HCC projects still rely on the reactive power control approach used for LCC systems. LCC achieves reactive power control by switching reactive power compensation devices, such as AC filters and shunt capacitors [17]. However, there is a risk of CF caused by switching reactive power compensation devices. For example, the Lingbao I converter station in China experienced 445 commutation failures from 2005 to 2022, of which 5% were caused by switching shunt capacitors [14]. Therefore, the reactive power control strategy needs further improvement.

Researches have been conducted for reactive power control strategies for different scenarios. In [18] and [19], a reactive power control method is proposed by co-operatively controlling the switched shunt devices and DC voltage. Although this method improves reactive power controllability at the LCC rectifier side of hybrid HVDC systems, it depends on the cable type, system strength, and other parameters. A coordinated reactive power control strategy based on adaptive voltage droop is proposed in [20]. This strategy can realize the dynamic voltage support for AC systems, however, there are stability issues in extremely weak grids. Besides, the above methods still require switching reactive power compensation devices, which may affect power systems' stable operation. Moreover, a large

number of reactive power compensation devices occupy a large area of converter stations and have high costs. A reactive power control method for low-power operation is proposed in [21], which improves reactive power consumption by increasing the extinction angle. However, this method cannot provide reactive power support for AC systems. In [22], a constant reactive power control strategy is proposed for suppressing the transient overvoltage caused by CF. However, the mechanism of consequential CF requires further analysis. Although the methods in [21] and [22] do not require switching reactive power compensation devices, they cannot provide reactive power support for AC systems and may not apply to HCC.

Research on reactive power control strategies for HCC remains limited. In [23], a control strategy for ultra-low reactive power operation of HCC is proposed by utilizing IGCTs' active turn-off and bidirectional voltage-withstanding capability. This strategy largely eliminates the extinction angle by improving the driving of IGCTs. However, the resulting extinction angle becomes so small that further engineering verification is needed to ensure its reliability.

In summary, the existing research has three key issues that need to be solved. First, reactive power should be regulated with minimal reliance on switching reactive power compensation devices to improve operation reliability. Second, reducing the reactive power demand during steady-state operation is essential to improve the economic efficiency of DC transmission systems. Third, reactive power support methods for AC systems suitable for HCC should be explored.

To address the issues mentioned above, a reactive power control strategy is proposed for small extinction angle operation of HCC, which is realized by the coordination of the converter transformer taps and extinction angles. The main contributions of the proposed strategy are as follows:

- 1) The proposed strategy can achieve reactive power regulation while maintaining constant active power. Instead of switching reactive power compensation devices, the proposed strategy only needs to adjust the transformer taps and coordinate with the extinction angle;
- 2) The proposed strategy can regulate reactive power in forward and reverse directions. Therefore, reactive power support for AC systems can be provided by controlling the HCC station to absorb less reactive power;
- 3) The theoretical rated extinction angle for HCC is proposed, which can reduce the reactive power demand. Compared to LCC using traditional reactive power control strategies, HCC using the proposed strategy has

higher economic efficiency.

The rest of this paper is organized as follows. In Section II, the topology and commutation principle of HCC are described. The reactive power control strategy for small extinction angle operation of HCC is proposed in Section III, while the theoretical adjustment capability under different rated extinction angles is also calculated, and a rated extinction angle recommended. Section IV presents simulation tests to verify the effectiveness and superiority of the proposed strategy. Finally, Section V concludes the paper.

## II. HCC COMMUTATION TECHNOLOGY

Before analyzing the reactive power control strategy of HCC, the topology and commutation principle of HCC are first elucidated.

### A. Topology of HCC

Taking a six-pulse converter as an example, the topological distinctions between the novel HCC and conventional LCC are shown in Fig. 1. In contrast to the thyristors employed in LCC, the HCC utilizes fully-controlled IGCTs, which are capable of active turn-off. The main branch of a HCC's bridge arm comprises IGCTs connected in series. Each IGCT is connected in parallel with an RC damping circuit for dynamic voltage equalization and a resistor for static voltage equalization. Unlike in LCC, an arrester is connected in parallel with two series connected IGCTs in HCC for managing additional stresses caused by the active turn-off of IGCTs. In addition, each HCC bridge arm is connected in parallel with an arrester to limit the electrical stress during the commutation process.

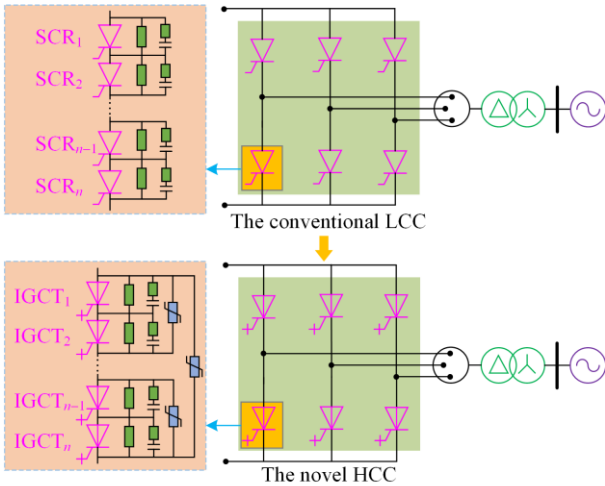


Fig. 1. Topologies of the conventional LCC and novel HCC.

Owing to the inability of thyristors to control their turn-off, LCC commutation relies entirely on AC voltage. Once the AC voltage decreases due to faults or disturbances, the normal commutation of LCC may be affected, leading to CF. In contrast, HCC can resist CF

by controlling the active turn-off of IGCTs and shorten the time for IGCTs to restore blocking ability after turn-off.

### B. Commutation Principle of HCC

HCC is called a hybrid commutation converter because its commutation mode includes natural and active commutation.

#### 1) Natural Commutation

Due to IGCTs being active turn-off devices, they cannot turn off naturally like thyristors when the current passing through it drops to zero. Therefore, the current and voltage of an IGCT can be monitored in real-time. If more than half of the IGCTs' current crosses zero in each bridge arm, a turn-off signal will be issued actively to achieve the natural turn-off. Since the active turn-off of IGCTs does not rely on the reverse recovery process required for thyristors, the blocking speed of IGCTs is faster than that of thyristors. Therefore, the feature is called IGCTs' recovery enhancement mode. This mode means that compared to LCC, HCC has the potential to operate at smaller extinction angles to reduce reactive power demand and converter station costs. The principle comparison with LCC under natural commutation is illustrated in Fig. 2.

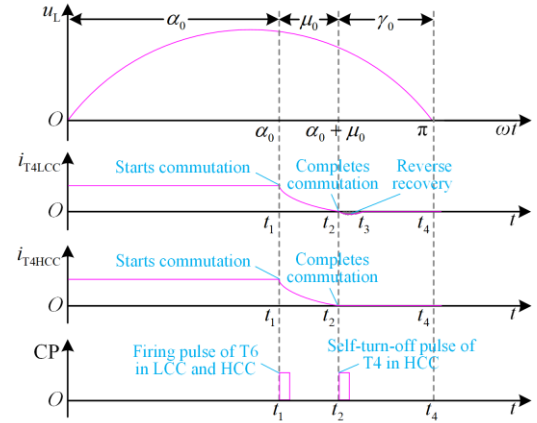


Fig. 2. The principle comparison with LCC under natural commutation.

As illustrated in Fig. 2, LCC undergoes a reverse recovery process following the zero-current crossing. For HCC, due to the detection of current crossing zero by the IGCT drive circuits, a reverse voltage can be applied to the gate and cathode of IGCTs, greatly reducing the time required to restore their blocking ability. The reverse recovery time in HCC is sufficiently short to be considered negligible, and its impact on the conclusions of this study is therefore insignificant.

#### 2) Active Commutation

In addition to the recovery enhancement mode,

IGCTs also have a commutation enhancement mode, which contributes to the active commutation of HCC. IGCTs can forcibly turn off the current that is flowing. Therefore, when the commutation capability is insufficient, an active turn-off command can be issued to turn off the bridge arm, thereby avoiding CF. The principle comparison with LCC under active commutation is shown in Fig. 3.

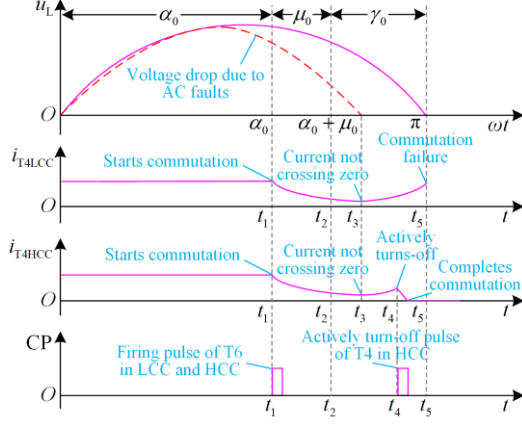


Fig. 3. The principle comparison with LCC under active commutation.

As evident from the analysis, when AC voltage depression occurs due to system faults, the current in bridge arm 4 of the LCC fails to reach zero before the AC voltage reverses polarity, leading to CF. In contrast, for HCC, an active signal is issued to turn off the commutation bridge arm, and the bridge arm current is forced to drop to zero to active commutation, thereby preventing CF.

### III. REACTIVE POWER CONTROL STRATEGY FOR HCC

#### A. Mechanism Analysis of Reactive Power Control

For HCC systems, the converter station absorbs reactive power in both rectifier and inverter states. The reactive power consumption can be obtained by the following equations:

$$Q_C = P_{dc} \tan \varphi \quad (1)$$

$$\tan \varphi = \sqrt{\left(\frac{N_{\text{bridge}} U_{\text{dio}}}{U_{\text{dc}}}\right)^2 - 1} \quad (2)$$

$$P_{dc} = U_{\text{dc}} I_{\text{dc}} \quad (3)$$

where  $Q_C$  is the reactive power consumption by HCC stations;  $P_{dc}$  is the active power;  $\varphi$  is the power factor angle;  $N_{\text{bridge}}$  is the number of six-pulse bridges connected in series;  $U_{\text{dio}}$  is the ideal no-load DC voltage;  $U_{\text{dc}}$  is the DC voltage; and  $I_{\text{dc}}$  is the DC current.

Equations (1)–(3) can be combined to obtain another expression of reactive power consumption:

$$Q_C = \sqrt{(N_{\text{bridge}} U_{\text{dio}} I_{\text{dc}})^2 - P_{dc}^2} \quad (4)$$

As indicated by (4), the reactive power consumption of the converter station is related to  $I_{\text{dc}}$ ,  $U_{\text{dio}}$ , and  $P_{dc}$ . Taking the derivative of  $I_{\text{dc}}$  on both sides of (4) yields:

$$\frac{dQ_C}{dI_{\text{dc}}} = \frac{(N_{\text{bridge}} U_{\text{dio}})^2 I_{\text{dc}}}{\sqrt{(N_{\text{bridge}} U_{\text{dio}} I_{\text{dc}})^2 - P_{dc}^2}} \quad (5)$$

From (5), it can be seen that  $dQ_C/dI_{\text{dc}}$  is greater than 0. According to the steady-state mathematical model of HVDC systems, it can be concluded that:

$$U_{\text{dc}} = N_{\text{bridge}} (U_{\text{dio}} \cos \gamma - 3X_T I_{\text{dc}}/\pi) \quad (6)$$

where  $\gamma$  is the extinction angle of the HCC inverters; and  $X_T$  is the commutation reactance.

As shown in (4), the reactive power consumption of the converter station can be controlled by adjusting  $I_{\text{dc}}$ . From (6),  $I_{\text{dc}}$  can be adjusted by changing the extinction angle  $\gamma$ .

For a single-pole six-pulse converter, the change in reactive power consumption of the inverter station when  $\gamma$  changes is further discussed. Equation (6) can be changed to:

$$U_{\text{dc}} = U_{\text{dio}} \cos \gamma - 3X_T I_{\text{dc}}/\pi \quad (7)$$

Then,  $P_{dc}$  can be expressed as:

$$P_{dc} = U_{\text{dc}} I_{\text{dc}} = U_{\text{dio}} \cos \gamma I_{\text{dc}} - 3X_T I_{\text{dc}}^2/\pi \quad (8)$$

Therefore,  $I_{\text{dc}}$  can be further solved by:

$$I_{\text{dc}} = \frac{U_{\text{dio}} \cos \gamma - \sqrt{(U_{\text{dio}} \cos \gamma)^2 - 12P_{dc}X_T/\pi}}{6X_T/\pi} \quad (9)$$

By taking the derivative of  $\gamma$  on both sides of (9), there is:

$$\frac{dI_{\text{dc}}}{d\gamma} = \frac{U_{\text{dio}} \sin \gamma}{6X_T/\pi} \times \left( \frac{U_{\text{dio}} \cos \gamma}{\sqrt{(U_{\text{dio}} \cos \gamma)^2 - 12P_{dc}X_T/\pi}} - 1 \right) \quad (10)$$

From (10), it can be seen that  $dI_{\text{dc}}/d\gamma$  is greater than 0. Therefore, the relationship between reactive power consumption and extinction angle can be obtained:

$$\frac{dQ_C}{d\gamma} = \frac{dQ_C}{dI_{\text{dc}}} \times \frac{dI_{\text{dc}}}{d\gamma} > 0 \quad (11)$$

As indicated by (11), the reactive power consumption of the inverter station is a monotonically increasing function of the extinction angle  $\gamma$ . Specifically, as  $\gamma$  increases, the reactive power consumption of the inverter station also increases. Therefore, the  $\gamma$  value of HCC can be used as a control variable to design the reactive power control strategy for HCC.

#### B. The Proposed Reactive Power Control Strategy

According to the external characteristics of HCC inverters,  $U_{\text{dc}}$  can also be expressed as:

$$U_{dc} = N_{\text{bridge}} (1.35E \cos \gamma - 3X_T I_{dc} / \pi) \quad (12)$$

where  $E$  is the valid value of no-load line voltage on the valve side of the converter transformer, and  $E \approx U_{\text{dio}} / 1.35$ .

The reactive power consumption of HCC inverters can also be expressed as:

$$Q_C = P_{dc} \tan \varphi = U_{dc} I_{dc} \sqrt{\left( \frac{N_{\text{bridge}} U_{\text{dio}}}{U_{dc}} \right)^2 - 1} \quad (13)$$

According to (12), assuming  $E$  remains constant, adjusting  $\gamma$  of HCC will cause changes in  $U_{dc}$  and  $I_{dc}$ . According to (13), for maintaining  $P_{dc}$  constant,  $Q_C$  can be adjusted by  $U_{\text{dio}}$ , which depends on the tap of the converter transformer. This analysis reveals that during steady-state operation, if it is necessary to adjust the reactive power exchange  $\delta Q_C$  between HCC and AC system while maintaining the same operation mode, the idea of coordinating the tap and  $\gamma$  can be adopted. Therefore, the reactive power control strategy is proposed, as shown in Fig. 4. The specific process is described as follows.

1) Initialization: Following the determination of main circuit parameters, the correlation between transformer tap positions and  $\delta Q_C$  is computationally established. This relationship is subsequently tabulated and integrated into the reactive power control algorithm as a reference database.

2) Reactive power: The actual  $\delta Q_C$  is monitored in real-time. When  $\delta Q_C$  surpasses predefined operational thresholds, the system automatically adjusts the transformer tap position according to the pre-established correlation table. Then,  $U_{\text{dio}}$  changes with the tap, and  $Q_C$  is adjusted.

3) Active power: The modification of  $U_{\text{dio}}$  inherently affects  $U_{dc}$ ,  $I_{dc}$ , and  $P_{dc}$ . Then, the constant current controller will detect the current deviation and adjust  $\gamma$  to ensure  $U_{dc}$ ,  $I_{dc}$ , and  $P_{dc}$  remain stable.

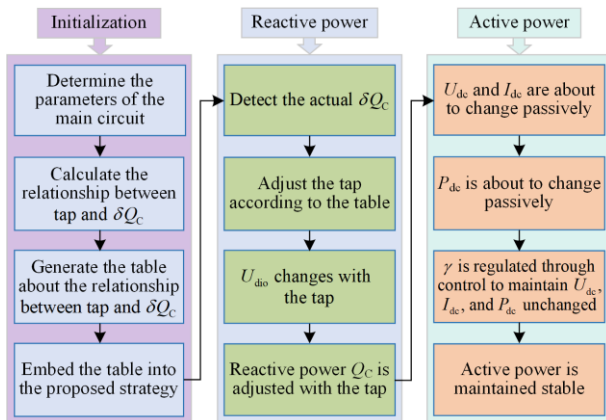


Fig. 4. The flowchart of the proposed control strategy.

### C. Calculation under Different Rated Extinction Angles

For quantitatively analyzing the correspondence relationship between the tap and  $\delta Q_C$  of HCC, the equivalent circuit on the AC/DC side is established, as shown in Fig. 5.

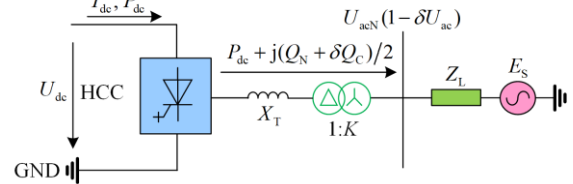


Fig. 5. The equivalent circuit on the AC/DC side.

In Fig. 5,  $Q_N$  and  $\delta Q_C$  are the rated reactive power and reactive power exchange of a double-pole HCC;  $K$  is the transformer ratio;  $U_{\text{acN}}$  is the rated AC bus voltage;  $\delta U_{\text{ac}}$  is the change in AC bus voltage; and  $P_{dc}$  is the active power of a single-pole HCC. The HCC consists of four six-pulse bridges connected in series to form a single-pole converter. The mathematical model of the HCC AC/DC side can be expressed as follows:

$$\begin{cases} U_{\text{dio}} = \frac{3\sqrt{2}}{K\pi} U_{\text{acN}} (1 - \delta U_{\text{ac}}) \\ K = K_N (1 + \delta K_{\text{pu}} \times T_k) \\ U_{dc} = N_{\text{bridge}} \left( U_{\text{dio}} \cos \gamma - \frac{3}{\pi} X_T I_{dc} \right) \\ \frac{Q_N + \delta Q_C}{2} = P_{dc} \sqrt{\left( \frac{N_{\text{bridge}} U_{\text{dio}}}{U_{dc}} \right)^2 - 1} \\ P_{dc} = U_{dc} I_{dc} \\ \delta U_{\text{ac}} = \frac{\delta Q_C}{S_{\text{ac}} - \sum Q_C} \\ \sum Q_C = Q_N \end{cases} \quad (14)$$

where  $K_N$  is the rated transformer ratio;  $\delta K_{\text{pu}}$  is the tap step, and  $\delta K_{\text{pu}} = 1.25\%$ ;  $T_k$  is the tap position;  $S_{\text{ac}}$  is the capacity of the AC system; and  $\sum Q_C$  is the total capacity provided by reactive power compensation equipment.

In (14), there are seven equations and ten state variables, including  $U_{\text{dio}}$ ,  $\delta U_{\text{ac}}$ ,  $K$ ,  $T_k$ ,  $U_{dc}$ ,  $I_{dc}$ ,  $\delta Q_C$ ,  $P_{dc}$ ,  $\gamma$ , and  $Q_N$ . The operational state of the HCC converter can be uniquely determined when any three independent variables are specified as operation conditions.

Equation (14) can be solved by Newton's method. Key state parameters such as  $\delta Q_C$  and  $\gamma$  corresponding to different tap positions under different rated extinction angles  $\gamma_N$  are obtained. Three typical  $\gamma_N$  of

17°, 12°, and 7° are selected for calculation. The results are as follows.

1) *Rated Extinction Angle*  $\gamma_N = 17^\circ$

If  $\gamma_N = 17^\circ$ ,  $U_{dio}$  of the HCC converter is:

$$U_{dio} = \frac{U_{dc}/N_{bridge} - U_T}{\cos \gamma_N - (d_{xN} - d_{rN})} = 230.8656 \text{ kV} \quad (15)$$

where  $U_T$  is the voltage drop of the IGBTs in conducting states;  $d_{xN}$  is the relative inductive voltage drop; and  $d_{rN}$  is the relative resistive voltage drop.

The commutation reactance  $X_T$  can be calculated as:

$$X_T = \frac{\pi d_{xN} U_{dio}}{3I_{dc}} = 4.3517 \ \Omega \quad (16)$$

The rated reactive power  $Q_N$  of HCC under  $\gamma_N = 17^\circ$  is:

$$Q_N = P_{dc} \sqrt{\left(\frac{N_{bridge} U_{dio}}{U_{dc}}\right)^2 - 1} = 4612.8 \text{ Mvar} \quad (17)$$

The rated transformer ratio  $K_N$  is calculated as:

$$K_N = \frac{3\sqrt{2}U_{acN}}{\pi U_{dio}} = 3.071 \quad (18)$$

It should be noted that the range of  $\gamma$  is 0°–25°. The relationship between reactive power adjustment capability and tap position under  $\gamma_N = 17^\circ$  is calculated as shown in Table I.

TABLE I  
THE RELATIONSHIP BETWEEN REACTIVE POWER ADJUSTMENT CAPABILITY AND TAP POSITION UNDER  $\gamma_N = 17^\circ$

Tap	$U_{dio}$ (kV)	$\delta U_{ac}$ (%)	$\gamma$ (°)	$Q_N$ (Mvar)	$\delta Q_C$ (Mvar)
-7	246.2	2.70	26.3	4612.8	1128.4
-6	243.8	2.31	25.0	4612.8	965.4
-5	241.5	1.92	23.9	4612.8	803.3
-4	239.3	1.54	22.7	4612.8	641.8
-3	237.1	1.15	21.4	4612.8	481.0
-2	235.0	0.77	20.0	4612.8	320.5
-1	232.9	0.38	18.6	4612.8	160.2
0	230.9	0.00	17.0	4612.8	0.0
1	228.9	-0.38	15.3	4612.8	-160.3
2	227.0	-0.77	13.4	4612.8	-320.9
3	225.1	-1.15	11.2	4612.8	-482.0
4	223.3	-1.54	8.6	4612.8	-643.9
5	221.5	-1.93	4.6	4612.8	-806.8
6	219.7	-2.32	0.0	4612.8	-971.0

As evidenced by the data presented in Table I, the increase in tap position leads to gradual decrease of  $U_{dio}$ . Furthermore, the reactive power consumption gradually decreases, and the AC bus voltage gradually increases. The extinction angle also gradually decreases.

When  $\gamma_N = 17^\circ$ , the proposed strategy can increase the consumption by 965.4 Mvar with a tap of -6, while reduce the consumption by 806.8 Mvar with a tap of 5. For each adjustment of the tap position, the AC bus voltage changes by about 0.4%, and the reactive power changes by about 160 Mvar.

2) *Rated Extinction Angle*  $\gamma_N = 12^\circ$

If  $\gamma_N = 12^\circ$ ,  $U_{dio}$ ,  $X_T$ ,  $Q_N$ , and  $K_N$ , calculated by (15)–(18), are 225.1878 kV, 4.2447  $\Omega$ , 4139.5 Mvar, and 3.1485, respectively. The relationship between the reactive power adjustment capability and tap position under  $\gamma_N = 12^\circ$  is calculated as shown in Table II.

The data presented in Table II demonstrates consistent behavioral patterns with those observed in Table I, maintaining identical trends in electrical parameter variations. When  $\gamma_N = 12^\circ$ , the proposed strategy increases absorption by 1333.0 Mvar with a tap of -8, and reduces consumption of 336.7 Mvar with a tap of 2. For each adjustment of the tap position, the AC bus voltage also changes by about 0.4%, and the reactive power changes by about 167 Mvar.

TABLE II  
THE RELATIONSHIP BETWEEN REACTIVE POWER ADJUSTMENT CAPABILITY AND TAP POSITION UNDER  $\gamma_N = 12^\circ$

Tap	$U_{dio}$ (kV)	$\delta U_{ac}$ (%)	$\gamma$ (°)	$Q_N$ (Mvar)	$\delta Q_C$ (Mvar)
-9	244.7	3.55	25.8	4139.5	1501.4
-8	242.3	3.15	24.6	4139.5	1333.0
-7	240.0	2.76	23.4	4139.5	1165.4
-6	237.7	2.36	22.1	4139.5	998.5
-5	235.5	1.97	20.7	4139.5	832.0
-4	233.3	1.58	19.2	4139.5	665.8
-3	231.2	1.18	17.7	4139.5	499.7
-2	229.1	0.79	16.0	4139.5	333.5
-1	227.1	0.40	14.1	4139.5	167.0
0	225.2	0.00	12.0	4139.5	0.0
1	223.3	-0.40	9.4	4139.5	-167.8
2	221.4	-0.80	5.9	4139.5	-336.7
3	219.7	-1.20	0.0	4139.5	-507.0

3) *Rated Extinction Angle*  $\gamma_N = 7^\circ$

If  $\gamma_N = 7^\circ$ , the calculated  $U_{dio}$ ,  $X_T$ ,  $Q_N$ , and  $K_N$  are 221.5953 kV, 4.1770  $\Omega$ , 3816.7 Mvar, and 3.1995, respectively. The relationship between the reactive power adjustment capability and tap position under  $\gamma_N = 7^\circ$  is calculated as shown in Table III.

As seen, when  $\gamma_N = 7^\circ$ , the proposed strategy can increase consumption by 1538.1 Mvar with a tap of -9. For each tap adjustment, the AC bus voltage changes by about 0.4%, and the reactive power changes by about 171 Mvar. Differently, when the tap position changes from 0 to 1,  $\gamma$  becomes 0, which is not allowed in real

application. Therefore, when  $\gamma_N = 7^\circ$ , the proposed strategy cannot absorb less reactive power to support AC systems.

TABLE III  
THE RELATIONSHIP BETWEEN REACTIVE POWER ADJUSTMENT CAPABILITY AND TAP POSITION UNDER  $\gamma_N = 7^\circ$

Tap	$U_{dio}$ (kV)	$\delta U_{ac}$ (%)	$\gamma$ ( $^\circ$ )	$Q_N$ (Mvar)	$\delta Q_C$ (Mvar)
-10	243.1	4.02	25.2	3816.7	1709.9
-9	240.7	3.61	24.0	3816.7	1538.1
-8	238.3	3.21	22.6	3816.7	1366.9
-7	236.0	2.81	21.3	3816.7	1196.3
-6	233.8	2.41	19.8	3816.7	1026.1
-5	231.6	2.01	18.3	3816.7	856.0
-4	229.5	1.61	16.6	3816.7	685.9
-3	227.4	1.21	14.8	3816.7	515.5
-2	225.4	0.81	12.7	3816.7	344.6
-1	223.5	0.41	10.2	3816.7	172.8
0	221.6	0.00	7.0	3816.7	0.0
1	219.8	-0.41	0.0	3816.7	-174.2

#### D. Analysis of Recommended Rated Extinction Angle

The flowchart in Section III.B demonstrates that the proposed reactive power control strategy can adjust reactive power while maintaining active power unchanged. Then, the recommended rated extinction angle when applying the proposed strategy is further analyzed. The selection criteria primarily consider two critical factors:

- 1) During steady-state operation, the rated reactive power demand at the rated extinction angle should be minimized as much as possible;
- 2) The total reactive power consumption should be minimized after applying the proposed strategy for reactive power adjustment.

In accordance with these criteria, the rated reactive power demand, reactive power support of the proposed strategy, and total reactive power consumption after adjustment are further calculated at various extinction angles, as shown in Fig. 6.

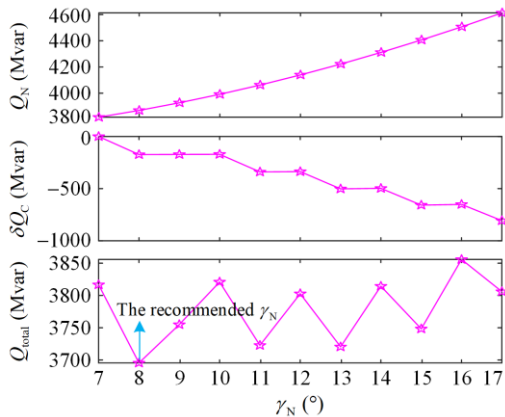


Fig. 6. Comparison of reactive power under various  $\gamma_N$ .

From Fig. 6, the post-adjustment total reactive power consumption reaches its minimum value at  $\gamma_N = 8^\circ$  and attains its maximum at  $\gamma_N = 16^\circ$ . Therefore, the theoretically recommended  $\gamma_N$  is  $8^\circ$ , while  $\gamma_N$  of  $16^\circ$  is not recommended. In addition, it is necessary to consider the ability to absorb reactive power comprehensively. The reactive power absorptions at various extinction angles are shown in Fig. 7.

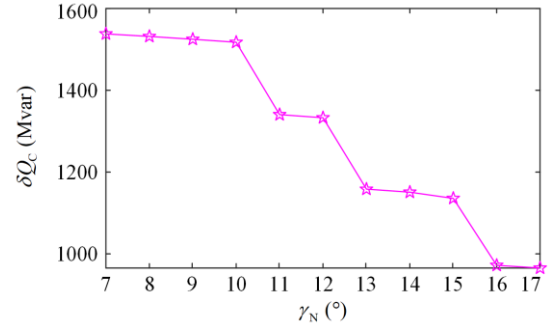


Fig. 7. The reactive power absorption adjusted by the proposed strategy at various extinction angles.

From Fig. 7, the smaller the rated extinction angle, the better the ability of the proposed strategy to absorb reactive power. Thus, the recommended rated extinction angle is chosen as  $8^\circ$ .

## IV. SIMULATION AND VERIFICATION

### A. Simulation System

#### 1) Test Model

To verify the effectiveness of the proposed reactive power control strategy, a four-terminal UHVDC simulation model is built in PSCAD/EMTDC, as illustrated in Fig. 8.

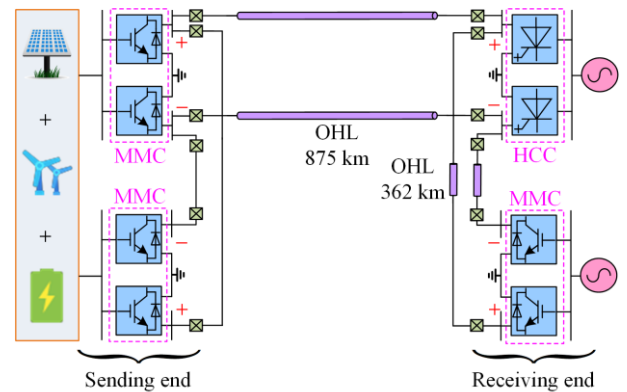


Fig. 8. Simulation model of four-terminal UHVDC.

The sending end of the model consists of two 100% renewable energy MMC stations, and the receiving end consists of one HCC station and one MMC station, respectively.  $V/f$  control is adopted at the two MMC stations at the sending end, and constant current control and voltage control are adopted at the HCC and MMC

stations at the receiving end, respectively. The lengths of the two sections of ultra-high voltage overhead lines (OHLs) are 875 km and 362 km, respectively.

## 2) Simulation Parameters

Given that HCC is the focus of this paper, the system parameters of the HCC are mainly introduced, as shown in Table IV, where  $N_{\text{pole}}$  is the number of poles;  $X_{\text{leakpu}}$  is the transformer leakage reactance;  $R_{\text{SC}}$  is the short circuit ratio; and  $S_{\text{filgroup}}$  is the capacity of a single filter group.

TABLE IV  
THE SYSTEM PARAMETERS

Parameters	Value	Parameters	Value
$U_{\text{dc}}$ (kV)	800	$U_{\text{T}}$ (kV)	0
$P_{\text{dc}}$ (MW)	8000	$S_{\text{ac}}$ (MVA)	46 406
$I_{\text{dc}}$ (kA)	5	$U_{\text{acN}}$ (kV)	525
$N_{\text{pole}}$	2	$\delta K_{\text{pu}}$ (%)	1.25
$N_{\text{bridge}}$	4	$R_{\text{SC}}$	5.8
$X_{\text{leakpu}}$	0.18	$S_{\text{filgroup}}$ (Mvar)	220

The simulation parameters corresponding to different rated extinction angles are different. According to (15),  $U_{\text{dio}}$  can be obtained at different rated extinction angles. Furthermore, equation (17) can be used to calculate  $Q_{\text{N}}$ , which can determine the capacity and number of reactive power compensation devices. According to (19), the rated voltage on the valve side can also be solved. The parameters under different rated extinction angles are shown in Table V, where  $U_{\text{VN}}$  is the rated voltage on the valve side;  $Q_{\text{filter}}$  is the capacity of AC filters; and  $N_{\text{filter}}$  is the number of AC filters in operation.

$$U_{\text{VN}} = \frac{\pi U_{\text{dio}}}{3\sqrt{2}} \quad (19)$$

TABLE V  
SIMULATION PARAMETERS UNDER DIFFERENT RATED EXTINCTION ANGLES

$\gamma_{\text{N}}$ (°)	$U_{\text{VN}}$ (kV)	$Q_{\text{filter}}$ (Mvar)	$N_{\text{filter}}$
17	170.9515	4620	21
12	166.7472	4180	19
7	164.0870	3740	17

## B. Simulation Result

In this section, the ability of the proposed strategy to adjust reactive power in both forward and reverse directions is verified under different  $\gamma_{\text{N}}$ . The forward direction refers to absorbing more reactive power, while the reverse direction refers to absorbing less reactive power.

### 1) Rated Extinction Angle $\gamma_{\text{N}} = 17^\circ$

The forward direction adjustment results at  $\gamma_{\text{N}} = 17^\circ$  are presented in Fig. 9. As the tap position changes from 0 to -6, the reactive power exchange  $\delta Q_{\text{C}}$  gradually changes from 167 Mvar to 1327 Mvar. The inverter absorbs an additional 1160 Mvar from the AC side, with an average reactive power exchange of 193 Mvar for each tap step. Meanwhile, the firing angle  $\alpha$  changes from  $109.2^\circ$  to  $105.9^\circ$ , and the extinction angle  $\gamma$  changes from  $17.2^\circ$  to  $24.9^\circ$ . It is generally considered that the upper limit of the extinction angle does not exceed  $25^\circ$ , so the simulation ends after the extinction angle exceeds  $25^\circ$ . Throughout the adjustment process,  $U_{\text{dc}}$  and  $P_{\text{dc}}$  maintain stable operation at 800 kV and 4000 MW, respectively. As the tap decreases, the reactive power absorbed from the AC side gradually increases, resulting in a gradual decrease in the AC bus voltage  $U_{\text{acRMS}}$ . The voltage decreased by 13 kV in six tap steps, with an average reduction of 2.2 kV per step. This accounts for about 0.4% of the rated AC voltage  $U_{\text{acN}}$ , which is consistent with the theoretical results.

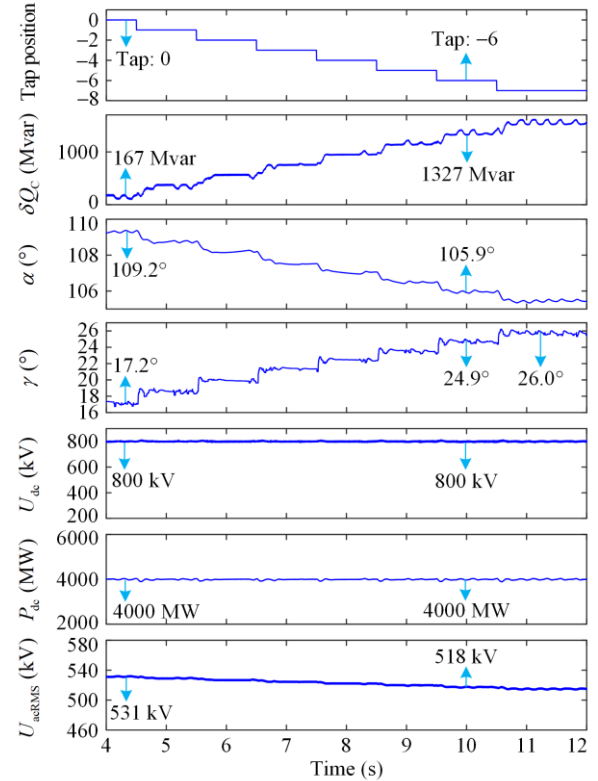


Fig. 9. The results of forward direction adjustment at  $\gamma_{\text{N}} = 17^\circ$ .

The reverse direction adjustment results at  $\gamma_{\text{N}} = 17^\circ$  are illustrated in Fig. 10. As the tap position gradually changes from 0 to 5, the reactive power exchange gradually changes from 167 Mvar to -874 Mvar, and

$\delta Q_C$  of the five tap steps is 1041 Mvar. On average, the converter absorbs 208 Mvar less from the AC side for each step.  $\alpha$  changes from  $109.2^\circ$  to  $112.0^\circ$ , and  $\gamma$  changes from  $17.2^\circ$  to  $6.6^\circ$ .  $U_{dc}$  and  $P_{dc}$  maintain 4000 MW and 800 kV. As the tap increases, the reactive power absorbed from the AC side decreases, causing the AC bus voltage to increase step by step. The variation per step is about 0.4% of  $U_{acN}$ , which is consistent with the theoretical results.

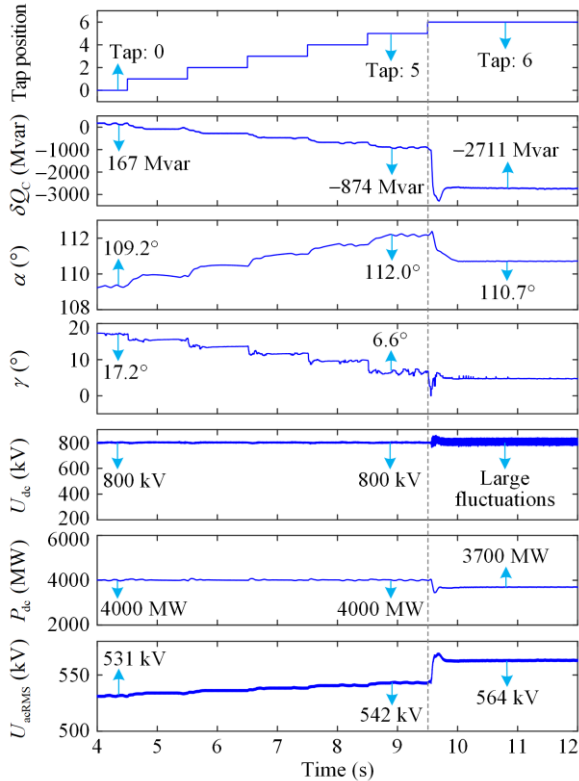


Fig. 10. The results of reverse direction adjustment at  $\gamma_N = 17^\circ$ .

When the tap position changes from 5 to 6,  $\gamma$  undergoes further reduction to maintain  $P_{dc}$  stability. Since  $\gamma$  becomes very small that it is below its lower limit in the model, resulting in abnormal measurements of  $\alpha$  and  $\gamma$ . Meanwhile,  $\delta Q_C$  and  $U_{acRMS}$  also undergo significant changes. The active power decreases, and there are large fluctuations in  $U_{dc}$ . Consequently, at  $\gamma_N = 17^\circ$ , the tap adjustment is operationally limited to five steps, achieving a maximum reactive power absorption reduction of 1041 Mvar while maintaining system stability.

## 2) Rated Extinction Angle $\gamma_N = 12^\circ$

The forward direction adjustment results at  $\gamma_N = 12^\circ$  are presented in Fig. 11. As the tap position progressively changes from 0 to -8,  $\delta Q_C$  gradually changes

from 134 Mvar to 1727 Mvar, representing a change of 1593 Mvar in eight steps. On average, the converter absorbs an additional 199 Mvar from the AC side for each step.  $\alpha$  changes from  $111.5^\circ$  to  $106.7^\circ$ , and  $\gamma$  changes from  $12.5^\circ$  to  $24.6^\circ$ .  $P_{dc}$  and  $U_{dc}$  operate smoothly at 4000 MW and 800 kV.  $U_{acRMS}$  decreases step by step, with each step decreasing by about 0.4% of  $U_{acN}$ .

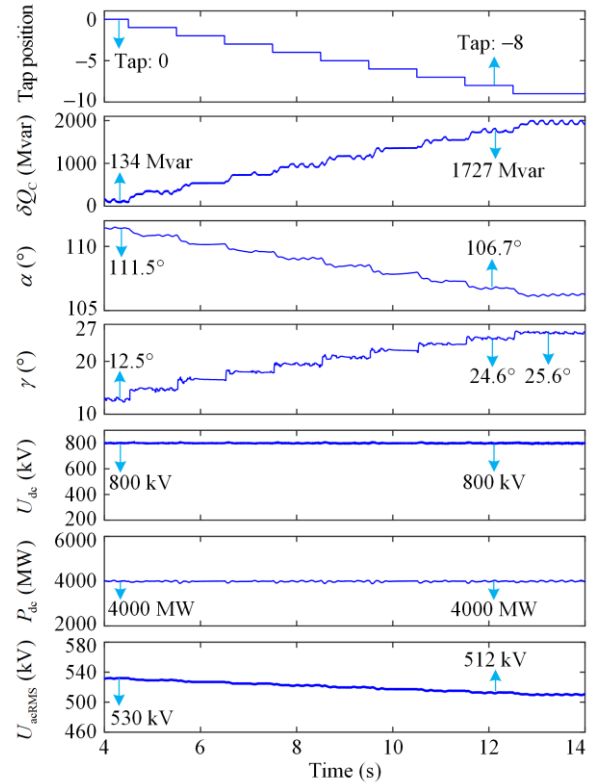
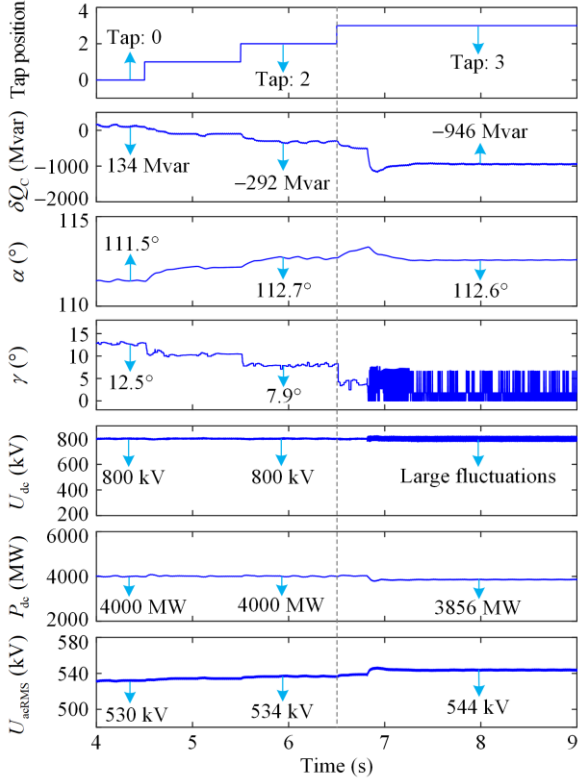


Fig. 11. The results of forward direction adjustment at  $\gamma_N = 12^\circ$ .

The reverse direction adjustment results at  $\gamma_N = 12^\circ$  are presented in Fig. 12. The tap position gradually changes from 0 to 2, and  $\delta Q_C$  gradually changes from 134 Mvar to -292 Mvar, accounting for a change of 426 Mvar in two steps. On average, the converter absorbs 213 Mvar less from the AC side for each step.  $\alpha$  changes from  $111.5^\circ$  to  $112.7^\circ$ , and  $\gamma$  changes from  $12.5^\circ$  to  $7.9^\circ$ .  $P_{dc}$  and  $U_{dc}$  still remain stable at their rated values.  $U_{acRMS}$  increases by about 0.4% of  $U_{acN}$  per step. When the tap position changes from 2 to 3,  $\gamma$  further decreases.  $\delta Q_C$  changes to -946 Mvar, and  $P_{dc}$  decreases.  $U_{dc}$  experiences large fluctuations, while  $U_{acRMS}$  experiences a significant increase. Therefore, when  $\gamma_N = 12^\circ$ , the tap can be adjusted up to two steps, which can reduce the absorption of reactive power by 426 Mvar.

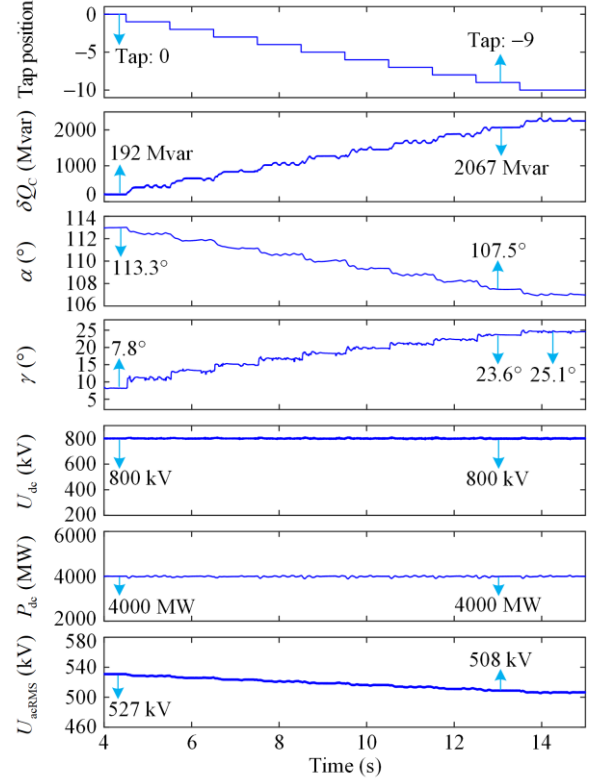
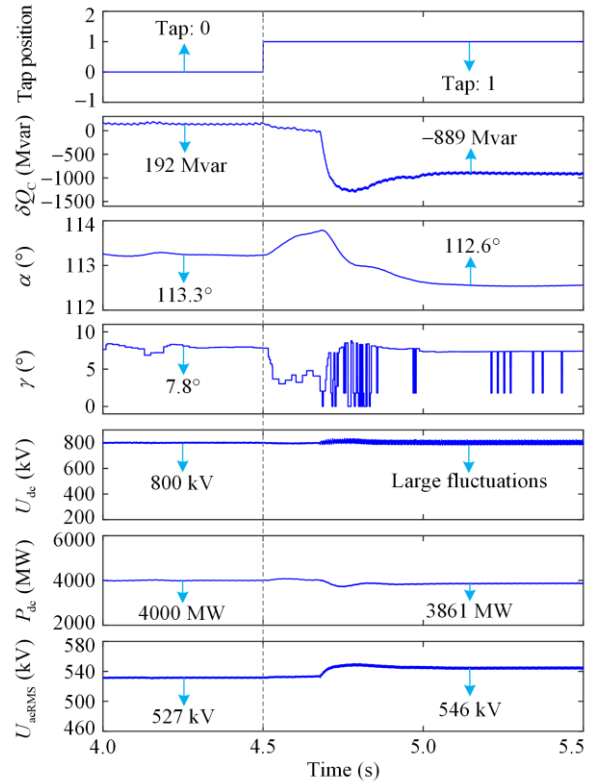

 Fig. 12. The results of reverse direction adjustment at  $\gamma_N = 12^\circ$ .

### 3) Rated Extinction Angle $\gamma_N = 7^\circ$

The forward direction adjustment results at  $\gamma_N = 7^\circ$  are presented in Fig. 13. Consistent with the aforementioned analysis,  $\delta Q_C$  changes by 1875 Mvar with tap changing by nine steps. The converter absorbs an additional 208 Mvar from the AC side for each step.  $\alpha$  changes from  $113.3^\circ$  to  $107.5^\circ$ , and  $\gamma$  changes from  $7.8^\circ$  to  $23.6^\circ$ .  $P_{dc}$  and  $U_{dc}$  remain stable, while  $U_{acRMS}$  decreases step by step, with each step decreasing by about 0.4% of  $U_{acN}$ . The reverse direction adjustment results at  $\gamma_N = 7^\circ$  are illustrated in Fig. 14.

In contrast to the previous scenarios, the tap is only adjusted by one step, and the measured  $\alpha$  and  $\gamma$  cannot maintain regular operation after a brief transition. Significant changes are made in  $\delta Q_C$  and  $U_{acRMS}$ .  $P_{dc}$  decreases, and there are large fluctuations in  $U_{dc}$ . Therefore, when  $\gamma_N = 7^\circ$ , the proposed strategy cannot provide reactive power support.

In summary, the proposed strategy can be utilized to increase or reduce reactive power absorption. The above simulation results verify the effectiveness of the proposed strategy. In particular, 1041 Mvar reactive power can be supported when  $\gamma_N = 17^\circ$  and 426 Mvar reactive power can be supported when  $\gamma_N = 12^\circ$ . When  $\gamma_N = 7^\circ$ , no reactive power can be supported by utilizing the proposed strategy.


 Fig. 13. The results of forward direction adjustment at  $\gamma_N = 7^\circ$ .

 Fig. 14. The results of reverse direction adjustment at  $\gamma_N = 7^\circ$ .

### C. Error Analysis

From Section III.C and Second IV.B, the reactive power consumption with five steps is reduced by

806.8 Mvar theoretically, while the simulation result is 1041 Mvar when  $\gamma_N = 17^\circ$ . Similarly, when  $\gamma_N = 12^\circ$ , the reactive power consumption is decreased theoretically by 336.7 Mvar after two steps, compared to the simulation result is 426 Mvar. Considering the rated reactive power of 4612.8 Mvar and 4139.5 Mvar, the errors are 1.02% and 1.08%, respectively, which are within the required 5% error range. The errors of  $\delta Q_C$  in the forward and reverse direction adjustments under different rated extinction angles are shown in Fig. 15.

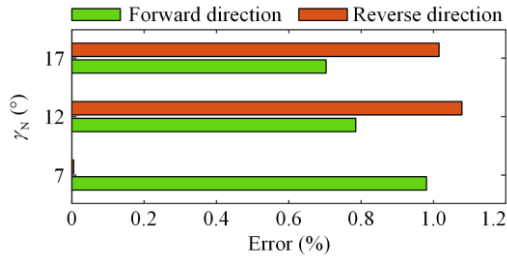


Fig. 15. The errors under different rated extinction angles.

It is evident that the errors in various situations are much lower than 5%. The reason for the error is that during the simulation analysis, the filters are added one by one, with 220 Mvar per group. Consequently, the capacity of the reactive power compensation device in operation cannot precisely equal to the converter's reactive power demand. In contrast, in theoretical analysis, the rated state is calculated based on  $\delta Q_C = 0$  Mvar, resulting in errors between the theoretical and simulation results. Nevertheless, the results are adequate since the errors are well within the required range.

#### D. Verification of Recommended Rated Extinction Angle

In Section III.D,  $8^\circ$  is selected as the recommended  $\gamma_N$ . The waveforms of various electrical quantities during steady-state operation at  $\gamma_N = 8^\circ$  are shown in Fig. 16. When  $\gamma_N = 8^\circ$ , the DC voltage and active power can remain stable at the rated values. Moreover, the voltage and current waveforms of the bridge arm are normal, and there is no CF.

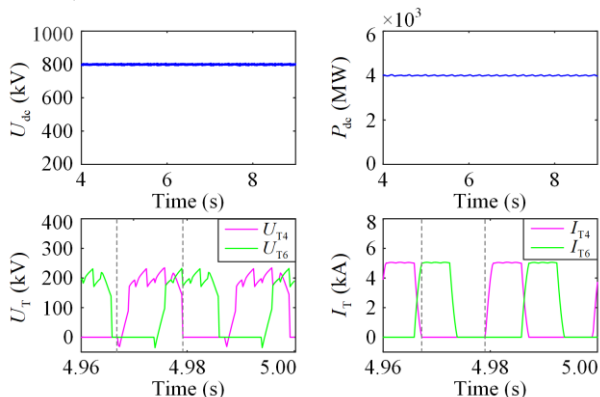


Fig. 16. Waveforms of key electrical quantities at  $\gamma_N = 8^\circ$ .

#### E. Superiority Analysis

There is almost no research on reactive power control strategies for HCC in existing studies. In addition, the reactive power control strategy of LCC is still used in the current HCC project. Therefore, to further highlight the advantages of the proposed strategy, comparisons are made between the proposed strategy for HCC and the traditional strategy of LCC, as shown in Fig. 17. The specific explanations are as follows.

##### 1) Rated Extinction Angle $\gamma_N$

The traditional reactive power control strategy applied to LCC typically has a rated extinction angle of  $17^\circ$ . However, the proposed strategy applied to HCC can operate at a reduced rated extinction angle of  $8^\circ$ , leading to lower reactive power consumption during steady-state operation.

##### 2) Cost Savings

A small group of AC filters typically have a cost ranging from  $\text{¥}5 \times 10^5$  to  $\text{¥}3 \times 10^6$ . Compared to the traditional strategy, the proposed strategy can reduce 4 groups of AC filters per phase at the same voltage and active power level. This means that the proposed strategy can save up to 36 million for three phases when compared to the traditional strategy, leading to better economic efficiency.

##### 3) Operation Reliability

The traditional strategy relies on switching reactive power compensation devices to adjust reactive power, which introduces CF risks. However, the proposed strategy can achieve reactive power adjustment through tap and  $\gamma$  coordination, with higher operation reliability. Furthermore, the inherent CF resistance of HCC further enhances the reliability of the proposed strategy.

##### 4) Reactive Power Demand

For 800 kV/8000 MW HVDC systems, LCC using the traditional strategy requires a reactive power consumption of 4612.8 Mvar at  $\gamma_N = 17^\circ$ . In comparison, HCC using the proposed strategy only requires 3868.5 Mvar at  $\gamma_N = 8^\circ$ . This represents a reduction in reactive power demand of approximately 800 Mvar, significantly improving the operating power factor of the DC transmission system.

##### 5) Cover Area

In LCC systems using the traditional control strategy, the AC filters occupy approximately 33% of the total converter station area. By contrast, HCC systems implementing the proposed strategy can have four fewer filter groups, reducing the cover area to 27%.

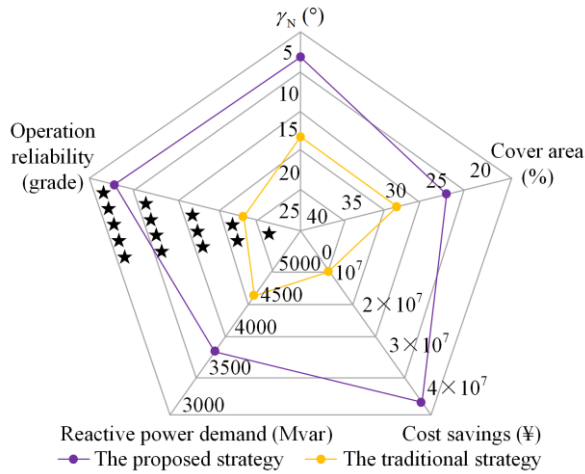


Fig. 17. Comparison with the traditional reactive power control strategy.

## V. CONCLUSION

In this paper, a reactive power control strategy is proposed for small extinction angle operation of HCC converter. The strategy has the following advantages.

1) Strong support capability: Compared with traditional strategies, the proposed strategy can improve the reactive power control capability of HCC, and provide reactive power support for weak AC power grids at the receiving end.

2) High reliability: Reactive power regulation can be achieved by adjusting the taps of converter transformers in conjunction with the extinction angle, avoiding frequent switching of reactive power compensation devices. Therefore, the proposed strategy further enhances the reliability of HCC systems, while HCC systems further increase the reliability due to the ability to withstand CF.

3) Significant economic efficiency: By supporting HCC operation at small extinction angles, the proposed strategy significantly reduces reactive power consumption. This reduction leads to substantial savings in converter station investment costs, making the strategy economically advantageous.

4) Wide applicability: The proposed strategy is implemented by analyzing the coupling mechanism between HCC and AC systems. Therefore, it is applicable to HCC-based two-terminal and multi-terminal DC transmission systems, as long as the HCC does not employ a constant extinction angle control.

The proposed strategy exhibits a relatively slow response speed, making it suitable primarily for steady-state reactive power regulation. Therefore, it cannot be applied to transient reactive power regulation in fault situations, which will be further studied in the

future work, alongside control and protection hardware-in-the-loop validation.

## ACKNOWLEDGMENT

Not applicable.

## AUTHORS' CONTRIBUTIONS

Jiaxing Ning: methodology, writing, software, and editing. Xiaoguang Wei: supervision and conceptualization. Zhichang Yuan, Longlong Chen, and Hui Du: methodology, review, and editing. Zhanqing Yu: supervision and conceptualization. All authors read and approved the final manuscript.

## FUNDING

This work is supported by Beijing Huairou Laboratory.

## AVAILABILITY OF DATA AND MATERIALS

Not applicable.

## DECLARATIONS

Competing interests: The authors declare that they have no known competing financial interests or personal relationships that could have appeared to influence the work reported in this article.

## AUTHORS' INFORMATION

**Jiaxing Ning** received the Ph.D. degree in electrical engineering with the Department of Electrical Engineering, Beijing Jiaotong University, Beijing, China, in 2023. Currently, he is working at Beijing Huairou Laboratory. His research interests include DC grid protection and control.

**Xiaoguang Wei** received the B.S. and M.S. degrees in electrical engineering from North China Electric Power University in 1999 and 2003, respectively, and the Ph.D. degree in electrical engineering from China Electric Power Research Institute (CEPRI) in 2010. He joined CEPRI in 2010, where he conducted research on line-commutated converter based high voltage DC (LCC-HVDC) transmission systems and DC breaker used in DC grid. Now, he is working at Beijing Huairou Laboratory. His research focus is on high-voltage silicon carbide (SiC) power electronic devices based on third-generation power semiconductor materials and the development of new converter equipment.

**Zhichang Yuan** received the B.E. and Ph.D. degrees in electrical engineering from Tsinghua University,

Beijing China, in 2001 and 2006, respectively. He is currently an associate professor with the Department of Electrical Engineering, Tsinghua University, where he has been since 2006. His research interests include power system stability analysis, FACTS, and battery storage.

**Longlong Chen** received B.S., M.S. and Ph.D degrees at Xi'an Jiaotong University, Huazhong University of Science and Technology and North China Electric Power University in 2007, 2009, and 2023, respectively. He used to work at China Electric Power Research Institute (CEPRI). Currently, he is with Beijing Huairou Laboratory. His research interests are DC circuit breakers and transmission line protection and control.

**Hui Du** received the B.S. degree in automation from North China Electric Power University, Beijing, China, in 2016. She received the M.S. degree in control theory and control engineering, and Ph.D. degree in electrical engineering, with the Department of Electrical Engineering, Wuhan University, Wuhan, China, in 2019 and 2023. Currently, she is working at Beijing Huairou Laboratory. Her research interests include HVDC transmission system operation and control.

**Zhanqing Yu** received the B.S. and Ph.D. degrees in electrical engineering from the Department of Electrical Engineering, Tsinghua University, Beijing, China, in 2003 and 2008, respectively. After graduation, he became a postdoctor, a lecturer, and an associate professor with the Department of Electrical Engineering, Tsinghua University in 2008, 2010, and 2012, respectively. He has participated in projects sponsored by High-Tech R&D Program (863 Program), National Basic Research Program of China (973 Program), and National Natural Science Foundation of China. His research interests include dc grid, dc breaker, electromagnetic environment, and electromagnetic compatibility.

#### REFERENCES

- [1] H. Shu, S. Wang, and S. Lei, "Single-ended protection method for hybrid HVDC transmission line based on transient voltage characteristic frequency band," *Protection and Control of Modern Power Systems*, vol. 8, no. 2, pp. 1-11, Apr. 2023.
- [2] Y. Li, N. Jia, and J. He *et al.*, "Non-unit protection scheme based on cooperation with control strategy for multiterminal hybrid HVDC system without line boundary," *Protection and Control of Modern Power Systems*, vol. 10, no. 5, pp. 41-55, Sep. 2025.
- [3] M. Barnes, D. Hertem, and S. Teeuwssen *et al.*, "HVDC systems in smart grids," *Proceedings of the IEEE*, vol. 105, no. 11, pp. 2082-2098, Nov. 2017.
- [4] Z. Liu, H. Gao, and S. Luo *et al.*, "A fast boundary protection for an AC transmission line connected to an LCC-HVDC inverter station," *Protection and Control of Modern Power Systems*, vol. 5, no. 4, pp. 1-12, Oct. 2020.
- [5] J. Ouyang, X. Pan, and J. Ye *et al.*, "An improved prediction method of subsequent commutation failure of an LCC-HVDC considering sequential control response," *Protection and Control of Modern Power Systems*, vol. 8, no. 3, pp. 1-11, Jul. 2023.
- [6] Y. Tan, Y. Sun, and J. Lin *et al.*, "Revisit impedance-based stability analysis of VSC-HVDC system," *IEEE Transactions on Power Systems*, vol. 39, no. 1, pp. 1728-1738, Jan. 2024.
- [7] T. Zhang, J. Yao, and Y. Lin *et al.*, "Impact of control interaction of wind farm with MMC-HVDC transmission system on distance protection adaptability under symmetric fault," *Protection and Control of Modern Power Systems*, vol. 10, no. 2, pp. 83-101, Mar. 2025.
- [8] C. Ren, J. Liu, and X. Li *et al.*, "Optimal design of reverse blocking IGCT for hybrid line commutated converter," *IEEE Transactions on Power Electronics*, vol. 38, no. 11, pp. 13957-13965, Nov. 2023.
- [9] Z. Yu, Z. Wang, and C. Xu *et al.*, "Comprehensive physical commutation characteristic analysis and test of hybrid line commutated converter based on physics compact model of IGCT," *IEEE Transactions on Power Electronics*, vol. 38, no. 2, pp. 1924-1934, Feb. 2023.
- [10] B. Zhu, S. Chen, and Y. Yang *et al.*, "An isolated DC/DC converter with bipolar output voltage self-balancing capability," *Power System Protection and Control*, vol. 53, no. 19, pp. 139-150, Oct. 2025. (in Chinese)
- [11] K. Jia, K. Liu, and T. Bi *et al.*, "Research on single-ended protection of a flexible HVDC transmission line based on waveform matching," *Power System Protection and Control*, vol. 53, no. 3, pp. 13-26, Feb. 2025. (in Chinese)
- [12] C. Xu, Z. Yu, and B. Zhao *et al.*, "Hybrid line commutated converter with fast commutation characteristic based on IGCT for HVDC application: topology, design methodology, and experiments," *IEEE Transactions on Power Electronics*, vol. 38, no. 4, pp. 4668-4679, Apr. 2023.
- [13] C. Ren, J. Pan, and J. Liu *et al.*, "Improving dv/dt immunity of reverse blocking IGCT for hybrid line-commutated converter," *IEEE Transactions on Power Electronics*, vol. 39, no. 4, pp. 4001-4005, Apr. 2024.
- [14] S. Wang, L. Qu, and Z. Zi *et al.*, "Commutation failure resistance strategy and RTDS verification of hybrid commutation converter," *Advanced Technology of Electrical Engineering and Energy*, vol. 43, no. 7, pp. 51-59, Jul. 2024. (in Chinese)
- [15] C. Xu, Z. Yu, and Z. Chen *et al.*, "Comprehensive analysis and experiments of RB-IGCT, IGCT with fast

- recovery diode and standard recovery diode in hybrid line-commutated converter for commutation failure mitigation,” *IEEE Transactions on Industrial Electronics*, vol. 70, no. 2, pp. 1126-1139, Feb. 2023.
- [16] C. Xu, Z. Yu, and B. Zhao *et al.*, “A novel hybrid line commutated converter based on IGCT to mitigate commutation failure for high-power HVDC application,” *IEEE Transactions on Power Electronics*, vol. 37, no. 5, pp. 4931-4936, May 2022.
- [17] Y. Xue and X. Zhang, “Reactive power and AC voltage control of LCC HVDC system with controllable capacitors,” *IEEE Transactions on Power Systems*, vol. 32, no. 1, pp. 753-764, Jan. 2017.
- [18] G. Lee, D. Kwon, and S. Moon *et al.*, “Reactive power control method for the LCC rectifier side of a hybrid HVDC system exploiting DC voltage adjustment and switched shunt device control,” *IEEE Transactions on Power Delivery*, vol. 35, no. 3, pp. 1575-1587, Oct. 2019.
- [19] G. Lee, P. Hwang, and S. Moon, “Reactive power control of hybrid multi-terminal HVDC systems considering the interaction between the AC network and multiple LCCs,” *IEEE Transactions on Power Systems*, vol. 36, no. 5, pp. 4562-4574, Feb. 2021.
- [20] X. Fan, Y. Chi, and Z. Wang, “Coordinated reactive power control for hybrid cascaded high-voltage direct-current links in weak AC grids,” *IET Generation, Transmission & Distribution*, vol. 18, no. 23, pp. 3788-3800, Dec. 2024.
- [21] X. Zhang, G. Cao, and C. Chen, “Proposal on reactive power control of HVDC system during low power transmission,” *Power System Technology*, vol. 36, no. 1, pp. 118-122, Jan. 2012. (in Chinese)
- [22] C. Yin and F. Li, “Reactive power control strategy for inhibiting transient overvoltage caused by commutation failure,” *IEEE Transactions on Power Systems*, vol. 36, no. 5, pp. 4764-4777, Mar. 2021.
- [23] C. Xu, Z. Yu, and B. Zhao *et al.*, “Ultra-low reactive power operation and control strategy of hybrid line commutated converter based on IGCT for HVDC application,” *IEEE Transactions on Industrial Electronics*, vol. 70, no. 12, pp. 12926-12932, Jan. 2023.